Accepted Manuscript

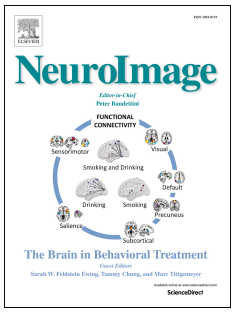

Prediction error connectivity: A new method for EEG state analysis

Alessandro Principe, Miguel Ley, Gerardo Conesa, Rodrigo Rocamora

PII: S1053-8119(18)32133-5

DOI: https://doi.org/10.1016/j.neuroimage.2018.11.052

Reference: YNIMG 15457

To appear in: *NeuroImage*

Received Date: 6 February 2018

Revised Date: 15 November 2018

Accepted Date: 27 November 2018

Please cite this article as: Principe, A., Ley, M., Conesa, G., Rocamora, R., Prediction error connectivity: A new method for EEG state analysis, *NeuroImage* (2018), doi: https://doi.org/10.1016/j.neuroimage.2018.11.052.

Prediction error connectivity: a new method for EEG state analysis

Authors and Affiliations

Alessandro Principe[1,2], Miguel Ley[1], Gerardo Conesa[2,3], Rodrigo Rocamora[1,2]

[1] Epilepsy Unit - Neurology dept. Hospital del Mar - Parc de Salut Mar - Barcelona, Spain

[2] IMIM - Hospital del Mar Medical Research Institute- Barcelona, Spain

[3] Neurosurgery Unit -Hospital del Mar - Parc de Salut Mar - Barcelona, Spain

Corresponding author: A. Principe - aprincipe@parcdesalutmar.cat

Abstract

Several models have been proposed to explain brain regional and interregional communication, the majority of them using methods that tap the frequency domain, like spectral coherence. Considering brain interareal communication as binary interactions, we describe a novel method devised to predict dynamics and thus highlight abrupt changes marked by unpredictability. Based on a variable-order Markov model algorithm developed in-house for data compression, the prediction error connectivity (PEC) estimates network transitions by calculating error matrices (EMs).

We analysed 20 hours of EEG signals of virtual networks generated with a neural mass model. Subnetworks changed through time (2 of 5 signals), from normal to normal or pathological states. PEC was superior to spectral coherence in detecting all considered transitions, especially in broad and ripple bands. Subsequently, EMs of real data were classified using a support vector machine in order to capture the transition from interictal to preictal state and calculate seizure risk. A single seizure was randomly selected for training. Through this approach it was possible to establish a threshold that the calculated risk consistently overcame minutes before the events. Using either spectral coherence or PEC we created 1000 models that successfully predicted 6 seizures (100% sensibility), a whole cluster recorded in a patient with hippocampal epilepsy. However, PEC resulted superior to coherence in terms of true seizure free time and amount of false warnings. Indeed, the best PEC model predicted 96% of interictal time (vs. 83% of coherence) of about 20 hours of stereo-EEG. This analysis was extended to patients with neo/mesocortical temporal, neocortical frontal, parietal and occipital lobe epilepsy. Again PEC showed high performance, allowing the prediction of 31 events distributed across 10 days with ROC AUCs that reached 98% (average 93±5%) in 6 different patients. Moreover, considering another state transition, PEC could classify and forecast up to 88% (average 85±3%) of the REM phase both in deep and scalp EEG.

In conclusion, PEC is a novel approach that relies on pattern analysis in the time-domain. We believe that this method can be successfully employed both for the study of brain connectivity, and also implemented in real-life solutions for seizure detection and prediction.

Keywords: coherence; Markov model; iEEG; EEG states; seizure prediction

1. Introduction

Despite medical treatment, about a third of epilepsy patients (around 0,3% of the world population) continue to have seizures (Kwan et Brodie, 2010). Since less than half of these patients are eligible for epilepsy surgery, it is necessary to devise alternative strategies for seizure control. The apparent random nature of ictal events is not only one of the most significant factors affecting patients' quality of life (Schulze-Bonhage et Kühn, 2008), but it is also a challenge for neuroscientists and physicians studying the brain dynamics related to this problem. In fact, since the 90s a huge effort has been made for solving seizure unpredictability, using a varied array of measures: correlation dimension and other fractal related measures, nonlinear similarity indexes, various types of frequential correlation and synchronization measures, compounded measures (for a comprehensive review see Mormann et al., 2007). Through these and other efforts aimed at understanding the basis of neural network behaviour, evidence has emerged of identifiable preictal brain states (for a comprehensive review see Stacey et al., 2011). Despite their reliable outcomes, early seizure forecasting methods were only recently implemented for real life solutions. Pitfalls were found not only in the methods themselves, but also in inadequate statistical analysis, especially the undersampling of the interictal period, which represents more than 99% of patients' time (Mormann et al., 2007; Andrzejak et al., 2009).

To define and quantify brain dynamics, published methods either use the raw EEG that is decomposed and represented in a multidimensional space (for chaos dynamics and nonlinear similarity methods) or preprocess the EEG into the frequency domain (correlation and synchronization methods). Indeed, the mainstream hypothesis of brain interareal communication is based on synchronisation of brain oscillations of the same or similar phase, and especially of high frequency activity (e.g. Rodriguez *et al.*, 1998; Palmigliano et al., 2017). This hypothesis increased the popularity of *spectral coherence* and related methods. In fact, their extensive usage is also justified by the observation that different brain regions present distinct oscillation behaviours that may become synchronous or dyssynchronous (e.g. Fell *et al.*, 2001; Matsumoto *et al.*, 2013). Other approaches that eminently focus on time and pattern sequence, like Markov chain models, have been widely employed for state analysis in information science (e.g. Ziv et Lempel, 1978), biology and genetics (e.g. Langmead et al., 2009). However, markovian methods have been less often used in scalp and invasive EEG (iEEG) studies with some exceptions, especially in the subfields of seizure prediction and detection (e.g. Santaniello *et al.*, 2011; Dadok *et al.*, 2015; Baldassano *et al.*, 2016). The general strategy behind most of approaches consists in calculating epoch similarity to a preictal phase or dissimilarity from an interictal phase, or both. Some approaches model and predict brain activity to compute this measures (e.g. in the works of Dadok and Baldassano), the majority use the distance between measures taken at preictal and interictal phases, assuming different levels of chaotic behaviour or synchronicity between brain areas.

Recently it has been demonstrated that seizure forecasting is possible (Brinkmann et al., 2015) but the classification between preictal and interictal time was very variable among patients, such that for some of them seizure warnings were issued for a considerable amount of daily time (Cook et al., 2013). Notwithstanding the usage of the latest machine learning technologies and problem solving modalities like crowdsourcing (Brinkmann et al., 2016), things did not change considerably. And even if this classification is methodologically plausible, most of promising algorithms require a large amount of processing time and memory. Most studies, even the ones using non-frequency domain methods, apply complex

transformation methods that need multiple iterations and require significant amounts of memory, especially when run for many sources like the EEG channels, (e.g. the Dirichlet process used in Baldassano et al., 2016).

In the current study, we introduce a novel method for EEG data analysis, entitled prediction error connectivity (PEC). PEC quantifies the error of brain regions as if they were failing to communicate with each other. The method relies on a very fast transform of the EEG signal and on a preprocessing phase with low memory requirements. Through the in-house developed variable-order Markov chain algorithm, the average weighted context (AWC), data streams are predicted bit by bit and the prediction error is considered. Unlike other approaches using data compression algorithms (e.g. Aarabi et He, 2012 and 2017), PEC uses the discrepancy between the predicted and the real data stream to infer state transitions. To our knowledge, this is the only method that uses the error made during prediction as a measure to detect changes in neural dynamics. To validate PEC, we first quantified the transitions in virtual data arranged in subnetworks that changed through time in a controlled way. Then we analysed real data recorded in patients with temporal, frontal, parietal and occipital lobe epilepsy. Finally, we also considered sleep stage transitions both in scalp and iEEG.

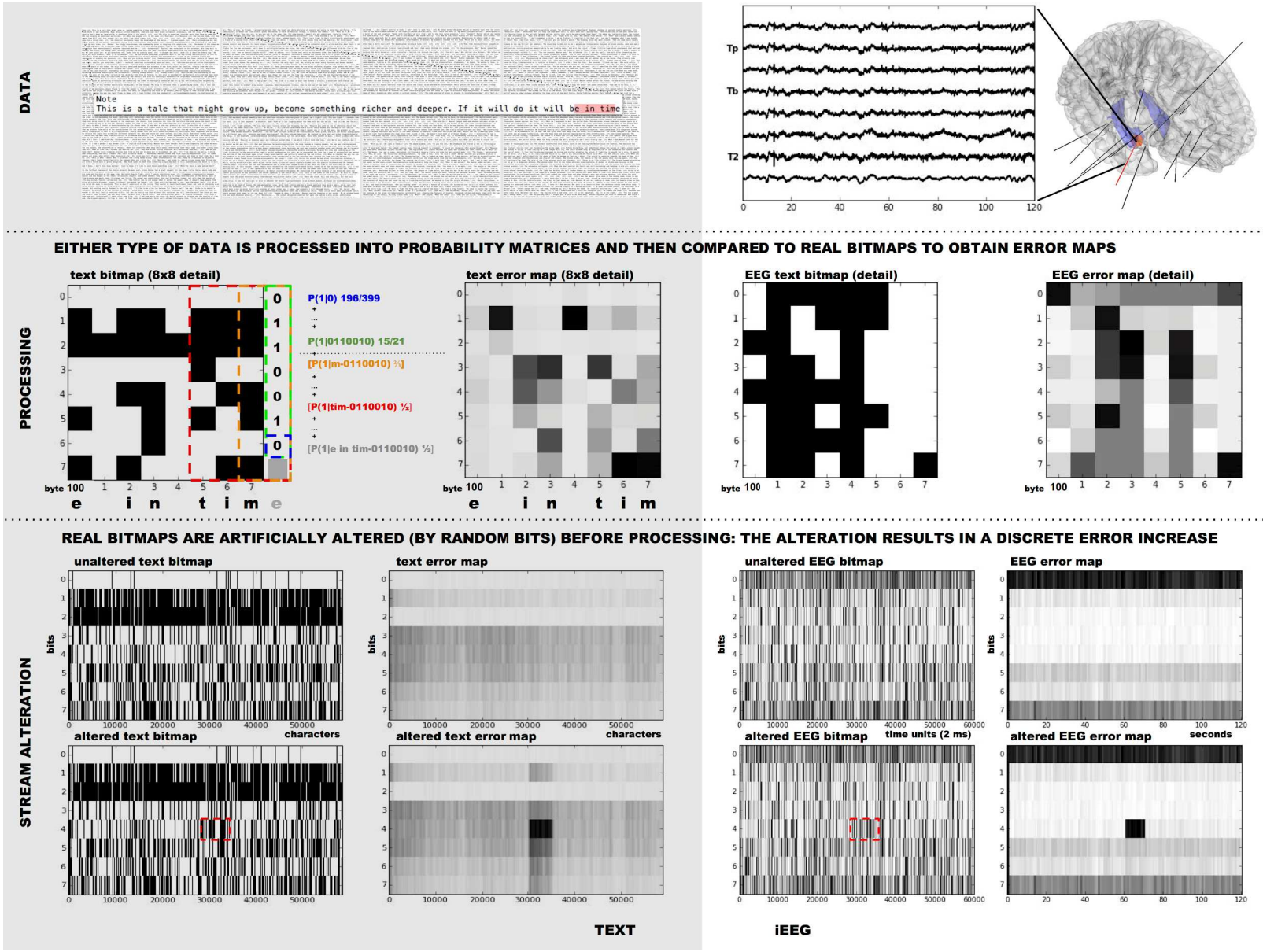

Figure 1. *Averaged Weighted Context (AWC) and bit stream prediction*. In the first line (**DATA**) we show an example of the data (TEXT, a text written by the first author, and a whole EEG epoch of 120 seconds) analysed by the algorithm (refer to section 2.1 for more information). In the second line (**PROCESSING**) we show raw 8x8 bit matrices (bitmaps, on the left in both TEXT and EEG boxes) and error maps of the same dimensions (on the right). In the TEXT box we show an example of AWC processing, which consists on averaging probabilities to find 1. Each probability equation example (blue, green, yellow and red) corresponds to a dotted box in the bitmap. Previous bit combinations are stored in memory as bit matches, which are retrieved through context keys. Dotted boxes represent the keys that retrieve multi-bit and byte match statistics (the grey equation corresponds to the last dictionary key, a 8x8+7 bit sequence that initialises a new match). Probabilities in square brackets correspond to byte probabilities (see section 2.1 for more information). In the third line (**STREAM ALTERATION**) we alter 5000 bits (10 seconds of iEEG at 500 Hz) from state 30000 on at position 4 in both data streams. We show raw bit streams (left, unaltered above, altered below) and error streams (right, corresponding to unaltered above, altered below). The analysis using AWC highlights the altered section as an increase of error values.

2. Materials and methods

2.1 Average Weighted Context (AWC)

Prediction error connectivity (*PEC*, see next section) was devised to work through a variable-order Markov model algorithm designed for pattern prediction, the additive weighted context (AWC). AWC produces good estimations of several types of data (see section supplementary results, 6.2, data compression experiments). In data compression, an estimation consists of bit forecasting from previous readings.

The iEEG as a sequence of bits. To use bit forecasting in the neurophysiological setting and characterise transitions of dynamics, first of all it was necessary to assess whether EEG data could be compared to data successfully processed by the AWC, like a text stream. Thus, given a text of around 60,000 characters, 120 seconds (at 500 Hz sampling rate) of interictal time were randomly selected from a patient undergoing an iEEG study (figure 1). Eight contacts (matching the 8 bits of text symbols) were chosen from an electrode targeting the epileptogenic zone. Although both text and iEEG were represented by a matrix of 8x60,000, the text matrix contained binary values, while the iEEG matrix floating point values. *Only the direction of the electrical vector was considered.* After this transform both matrices contained 8x60,000 bit values (bitmaps).

Forecasting sequences of bits to obtain error maps. *Bitmaps* are transformed by AWC into probability maps, then into *error maps*, $E = |P(B) - B|$ where *B* is the original bitmap and *P(B)* is the probability map.

What is the AWC probability map? The AWC transforms a sequence of bits into a sequence of probabilities that range from 0 to 1. Every map starts with a variable number of 0.5 values that depends on the number of new bit patterns encountered. Whenever the pattern at the current position matches a previously encountered pattern, the AWC computes the probability of the next bit instead of giving an output 0.5 (average probability). In other words, for new patterns the probability of the next bit is 0.5 (neither 0, nor 1), while for previously encountered patterns the probability is either close to 0 or 1.

How is the prediction of the next bit computed? To compute the probability of the next bit the AWC takes into account two dimensions: *space*, the number of bits that encode the message symbols (e.g. 8 bits or byte per text character); and *time*, the number of considered past symbols. Taken together, these two parameters make up the *context*. To compare text

and iEEG a context of 8x8 is used for simplicity. The context is implemented a set of bit patterns (keys) for retrieving the next bit statistics of previous matches. Considering an 8x8 context, the prediction starts with a key of 1 bit (previous bit), and it is extended bit by bit until a maximum of 7 bits, and then byte by byte until a maximum of 8x8+7 bits is reached. Finally, the context is shifted and the process starts again for the next pattern (a new character in the text stream, a new pattern of stacked electric vector directions in the iEEG). Despite a context of 8x8 implies a dictionary of $4.7 \cdot 10^{21}$ potential keys, in practice only a small fraction of them (a tree of patterns) is stored in memory, since keys become allocated only if found. Every key points to a *match*, which is a memory space that stores two values: the number of encountered 1s and the number of 0s and 1s, which in practice represents the times the bit pattern was found in previous readings.

How is the process step by step? In figure 1 the prediction of a bit of text data is represented. In the example the algorithm is shown at the position 100 (byte 100) that corresponds to the string 'e in tim' in the text. The algorithm has already computed the first 7 bits of the character 'e'. The prediction of the last bit consists in averaging the statistics of all previous matches starting from the 0-bit match. The 0-bit match is unbound and updated at every bit. After the 0-bit, the rest of multiple-bit matches are added up starting from 1-bit (196/399 in the example, blue in figure 1) up to the 7-bit match (15/21, green in figure 1). Finally, all symbol matches -bytes in a 8x8 context- are added up. For instance, considering the byte match 'm', 'me' appears twice in the words 'become' and 'something', while the letter 'm' appears 3 times (also in 'might'), therefore the sequence 'me' has a probability of ⅔ (orange in figure 1). On the other hand, since 'time' and 'e in time' never appear before their probability is set to ½ (average probability, red and grey in figure 1).

How are the statistics of frequent and infrequent matches balanced? All probabilities except the 0-bit are weighted in two ways: first, they are multiplied by a constant (the *training factor*, see section 6.1 in supplementary methods and results), then they are multiplied by a *length factor* that depends on the length of the key (long patterns appear less often than short ones). By this correction multiple-bit and byte matches are balanced against each other, and also against the 0-bit match, the most frequent since it is updated at every bit. Before applying the length correction, a *limiting function* is used to balance the most frequent patterns between each other, and also to minimise memory requirements (see section 6.1). Thus, the equation of next bit prediction is the following:

$$P(b\ \ _c) = \frac{m\ \ {}^{1}_{0} + \sum_{x=c}^{c-\beta} l(m\ \ {}^{1}_{x}k)(1+c-x) + \sum_{y=1}^{t} l(m\ \ {}^{1}_{c-\beta-ys}\,k)(1+\beta+y)}{m\ \ {}^{01}_{0} + \sum_{x=c}^{c-\beta} l(m\ \ {}^{01}_{x}k)(1+c-x) + \sum_{y=1}^{t} l(m\ \ {}^{01}_{c-\beta-ys}\,k)(1+\beta+y)}$$

where $P(b\ \ _c)$is the prediction of current bit *c*, *m* is a bit sequence up to bit *c* that points to a match (m^1 denotes the number of encountered 1, while m^{01} denotes the number of all previous matches), m_0 is the 0-bit match; *k* is the constant for balancing matches against m_0, while *l* is the function that limit the size of the most frequent matches; *s* is the current space and *t* is the current time; β represents the remainder of c/s or $c \bmod s$.

Error maps are used to detect dynamics changes. The chosen stream of iEEG channels was processed into an error map, which did not significantly differ from the error map obtained by a text stream (see Figure 1). Through the *stream alteration test* we assessed whether a random change of dynamics would increase the error rates, as expected. Since the AWC records bit occurrences after already encountered patterns, random bits should hamper bit prediction and thus increase the error where the alteration occurred. To check

this hypothesis we produced an artificial change of dynamics: we altered 5000 bits at bit 4 from byte 30.000 on, using sequences of 1-30 bits copied from random bit streams at random times, both in the text and iEEG streams (red dotted rectangles in figure 1). In both text and iEEG, the error dramatically rose from byte 30.000 on up to approximately 35.000, with a peak at bit 4 (see Figure 1).

2.2 Prediction error connectivity, signal processing and statistical analyses

Given that both text and EEG data could be processed into error maps that are reactive to dynamics changes (see 2.1), which should be the best number of EEG channels to analyse and in which order? Analysing several channels at the same time, like in figure 1, and all their possible combinations would require an unmanageable amount of time and memory, as reported in 2.1 (a context of 8x8 bits would produce $4.7 \cdot 10^{21}$ potential bit keys). For this reason, instead of analysing multiple contacts and relying on electrode placements to determine the best order, we decided to analyse *all possible contact pairs* or a subset of them. We implement this method in three steps: *binarization*, *serialization* and *online pattern analysis* (see figure 2). The method was implemented entirely in Python (version 3.6.1). The hybrid C/Python modules Numpy (Walt et al., 2011; version 1.13.0), Scipy (Jones et al., 2016; version 0.19.0) and Matplotlib (Hunter et al., 2007; version 2.1.0) were used for statistics, graphics, and for the calculation of coherence matrices (see below).

Binarization. The first step was the binary trending: the EEG data was transformed into a series of zeros and ones, using one when the previous sample was either equal or smaller than the current (see figure 2.B). This transformation maintains only the signal shape but loses the amplitude information. Other time series measures like permutation entropy consider discrete parts of the EEG, like its trend. We believed that this particular kind of reduction did not remove information about the temporal dynamics of the synaptic activity, which is the main source of the extracellular current flows that determine the electric vectors recorded by the EEG (Buzsáki et al., 2012). This is because the electric potential amplitude relates to the proximity of the source, therefore the flattening only reduces the information about the exact position of the various components of the signal, which in turn can be determined by temporal analysis.

Serialization. Considering two contacts, A and B, a new bit stream was made by putting in sequence the first bit of A and the first of B, then the second of A and the second of B, and so on. This process, which we called *serialization*, was used to check for synchronisation (see figure 2). By serialization, the two sources produced a single output. Therefore, if their variation was homogeneous the stream would become repetitive and predictable, thus suggesting related processes that worked synchronously. On the other hand, the unpredictability of the stream would indicate independent processes or a change in dynamics.

Online pattern analysis. The predictability was obtained through the AWC bit prediction (see 2.1, figure 1 and figure 2). A sliding window corresponding to an AWC with context 2x6 (the *space* -2- referred to the number of contacts, the *time* -6- was defined by compression studies, see section 6) walked along the serialized stream, predicting the next bit by recording pattern statistics. Pattern analysis operates *online* because the algorithm does not predict with forward knowledge, which would imply a readout phase followed by a prediction

phase. The AWC reads and predicts at the same time, with just a single read/predict passage. Practically, the AWC constructed trees of patterns, which are the sub sequences found by reading the stream. The statistics of pattern trees were used to predict the next bit by averaging incremental matches (see 2.1 and figure 1, PROCESSING). For further details about AWC memory management and statistics see section 6. As an important note, all experiments were done using bit statistics that never overcame 16 bits or 2 bytes. This limited the memory requirements to around 2 kilobytes per contact pair. Therefore, if the process is run pair by pair, 2 kilobytes is the minimum amount of memory needed.

Error matrices (EM). All possible combinations with duplicates were considered (e.g. following the example of figure 2, AA, AB, BA, BB) since the algorithms provides asymmetrical predictability values. The AWC returns the continuous prediction error that is used to create error matrices (EM), which are constructed as follows:

$$EM_{ab} = \underline{|P(B_{ab}) - B_{ab}|}$$

where *a* and *b* are the matrix row and column indices respectively, *P* is a function representing the transformation computed by the AWC, *B* is the bit sequence. As described above, each sequence was made of two bit streams and the AWC allowed a specific error retrieval, therefore we stored separately the error of the most and the less relevant (using big-endianness) bit sequence (0 and 1 respectively). For all calculations we used bit 1. Since bit 1 is the last predicted bit (the easiest to predict) we expected to find low error yields in a more predictable sequence. Therefore the effects of a change of dynamics, which decreases predictability, although altering both bits, would be more evident on bit 1.

Coherence matrices (CM). We compared the results with the normalized spectral density using a coherence matrix obtained with:

$$CM_{ab} = \frac{|P_{ab}|^2}{P_{aa} P_{bb}}$$

where *P* is the power spectral density by Welch's average periodogram method. EMs, like CMs, are sets of values ranging from 0 to 1. Since the AWC was written in pure Python, in order to compare processing times, CMs were partially implemented in pure Python (bypassing the accelerated routines of Numpy and Scipy).

Mann Whitney U and t-test were performed accordingly to distributions. To check for Gaussian distribution we used the Shapiro-Wilk normality test using random sampling when needed.

2.3 Neural mass model, virtual signals and network transitions

Twenty hours of virtual signals were generated using a neural mass model developed to produce virtual EEG signals from organized networks of neural populations (Wendling *et al.*, 2000). Among others (membrane average time constant, dendritic tree average time delays, average number of synaptic contacts of the feedback loops) the model uses two important parameters to generate EEG sources, the average excitatory and inhibitory synaptic gain. We modified the latter to produce networks that yielded signals with similar characteristics to

normal EEG activity, interictal-like (increased excitatory synaptic gain) and seizure-like activity (increased excitatory and decreased inhibitory synaptic gain). We used the standard values described by Wendling and colleagues with some exceptions: in normal signals we used 3.25 and 22 mV for average excitatory and average inhibitory synaptic gain respectively, in interictal-like signals we increased the average excitatory gain up to 4, variable until 8 mV, while in seizure-like signals we used an excitatory gain of 8 mV and decreased the inhibitory gain to 10 mV. The rest of the parameters were set to standard.

Virtual networks. We generated stationary (S) and variant (V) signals with a sampling rate of 500Hz to form networks with controlled linear transitions. Both S and V signals were produced using from 1 to 3 common sources and 1 to 3 extra sources, each source being a distinct neural mass. Variant signals used as many common sources as the stationary ones, though coupled with time-shifting extra sources. The extra sources were generated by waxing and waning several neural masses (from 1 to 3) in a linear fashion (source drift). We used the aforementioned neural mass parameters to build three types of network transitions: from normal to normal, from normal to interictal-like and from normal to seizure-like EEG signals. To simulate a focal transition, similar to the distribution of focal interictal activity or seizures, we constructed unevenly distributed epochs of 5 nodes per 60 seconds with 3 S and 2 V signals (see figure 3.A). In practice, networks of 5 nodes were generated simulating an iEEG recorded from 5 contacts. Of the 5 signals, 2 (V signals) linearly changed from a dynamic to another across 60 seconds.

Network transition detection. To obtain values of network transitions we constructed two EMs or two CMs per minute using the first and the last 30 seconds. We then computed the distance between matrices using:

$$\Delta = |X_{0-30s} - X_{30-60s}|$$

where X stands either for EMs or CMs. For the analysis we used broadband signals and the following sub-bands: δ-θ, α, β, γ and ripple (60-120 Hz), obtained through a butterworth bandpass filter.

2.4 Epilepsy patients and procedures

About 20 hours (1151 minutes) of stereotactic iEEG (SEEG) from a patient with pharmacoresistant motor cognitive seizures were analysed. The patient was identified in our centre among epilepsy surgery candidates who underwent SEEG evaluation for epilepsy surgery and was selected because she presented a cluster of 7 seizures and well defined focal seizure onset zone (SOZ). The subject was also selected because she was our first patient with hippocampal epilepsy explored with SEEG. A right hippocampal sclerosis was found on MRI recordings. SEEG exploration was performed, given a seizure semiology (with some opercular and insular characteristics) and an extensive PET hypometabolism, suggesting of temporal plus epilepsy (which indicates a complex epileptogenic network located within the temporal lobe and over neighbouring structures). To check whether the strategy could work in other epilepsy types, we chronologically included a non paleocortical temporal lobe, a frontal lobe, a parietal lobe and an occipital lobe epilepsy patient. All presented focal seizures with cognitive and/or motor symptoms. All but the patient with

occipital lobe epilepsy presented secondary tonic-clonic seizures. Refer to table 1 for clinical and electrode implants details.

Finally, to test extensibility to other state transitions and to surface EEG we included a sixth patient with a non-lesional left parietal lobe epilepsy. Despite the extensive bilateral mapping (16 electrodes, 15 on the left hemisphere), a good definition of the SOZ was not possible. The patient was also monitored with surface EEG electrodes. Refer to results for clinical information and electrode implants details.

All recordings were performed using a standard clinical EEG system (XLTEK, subsidiary of Natus Medical) with 500 Hz sampling rate. Implantations were performed using 5 to 16 (average 10) intracerebral electrodes (Dixi Médical, Besançon, France; diameter: 0.8 mm; 5 to 15 contacts, 2 mm long, 1.5 mm apart) that were stereotactically inserted using robotic guidance (ROSA, Medtech Surgical, Inc). The decision to implant, the selection of the electrode targets and the implantation duration were entirely made on clinical grounds without reference to this research study.

2.5 Classification analysis and seizure risk assessment

We classified EMs in order to obtain a value indicating the proximity of seizures. This process is depicted in figure 4.A. In the first step, *sampling*, 10 random samples of 1 minute of all EEG channels in the interictal (everything but preictal and ictal time) and 10 in the preictal time (5 to 10 minutes before the event) were processed into EMs. In order to obtain results in an acceptable lapse of processing time we used 120 random contiguous points of EEG downsampled at 62 Hz (2 seconds) per minute. One-hundred and twenty points represents 10 times the memory that the AWC uses with a 2x6 context. In the second step, *training*, we used a *support vector machine* (SVM) implemented in a hybrid C/Python library frequently used in machine learning problems (Scikit-learn; Pedregosa, 2011). SVMs are especially useful when the supervised classification involves binary choices and/or trees (Cortes, 1995). The SVM was trained to distinguish between interictal and preictal EMs by scoring them with 0 and 1 respectively. Using this *classification*, we computed continuous risk curves by scoring each minute of the EEG stream. Scores in a sliding buffer of 10 EMs were averaged to compute the curve: when all values were 0 then the average score was 0, which translates to *far from seizure*; instead when all values were 1, the average score was 1, thus indicating *maximal proximity* to an ictal event. The same procedure was repeated using CMs instead of EMs.

After this analysis, we assessed whether more events could be predicted by training the classifier with a single seizure. Two different epileptologists, AP and RR, selected three SOZ contacts of the patient with hippocampal epilepsy. To avoid statistical biases, continuous SEEG signals without resampling were used. To produce risk curves the SVM classifier was trained with random EMs and CMs selected in a preictal period of 3 to 5 minutes of a single seizure (preictal) and random EMs and CMs taken outside of any preictal and ictal period (interictal). Instead of using a buffer of 10 matrices we used only three. We discarded models that could not successfully recognise all ictal events by setting lowest thresholds. We repeated the procedure 1000 times and assessed: *true predicted seizure free time*, *number of false warnings* and *warning time*. We considered a warning to be true when lasting until an ictal event. Warnings could be retriggered (nested warnings) and, without retriggering, lasted at least a number of minutes equal to the chosen preictal training time (3 to 5 minutes). Again for this analysis we used EMs and CMs.

Finally, we extended the procedure to the remaining patients, again using unabridged minutes, full sampling rate, and three adjacent contacts lying in the same electrode targeting the SOZ. The SOZs were identified by three different epileptologists, AP, ML and RR. *True predicted seizure free time*, *number of false warnings* and *warning time* were evaluated. All models were assessed through receiver operator characteristic areas under the curve (ROC AUC). For this extension we used only EMs.

2.6 Risk assessment with downsampling and far from the SOZ

Three consecutive days (71.8 hours) recorded from deep electrode implants were used. Three adjacent contacts lying in the same electrode were selected as the closest to SOZ; three hippocampal contacts that did not present interictal activity were also chosen. Seizure start and end were identified by two different epileptologists, AP and ML. Data was processed into EMs, either unabridged at full sampling rate, and the first two seconds of each minute resampled at 62 Hz. As in 2.5 *true predicted seizure free time*, *number of false warnings* and *warning time* were evaluated. All models were assessed through receiver operator characteristic areas under the curve (ROC AUC).

2.7 Sleep phase transition classification

For this experiment we analysed data recorded from the same subject of 2.6. For sleep phase transition we used either three head hippocampal contacts (the same as in 2.6) and three surface EEG derivations placed over the non-epileptic hemisphere (F2-F8, F8-T2 and T2-T4, because of the electrode implants no full 10-20 montage was available). Ocular and chin contacts were present and used *only* for manual sleep classification. From lights off until lights on, 535 minutes were recorded. AP and RR staged sleep phases independently, then REM phases were selected. Unabridged minutes at full sampling rate (500 Hz) were processed in EMs. For REM stage classification we used the same framework used in 2.5 and 2.6, by considering non-REM to REM transitions instead of interictal to preictal phase transitions. Phases longer than 5 minutes were split into distinct adjacent events. A buffer of 3 matrices was again used. Similar to what was done in section 2.5, 1000 SVM models were built using 3 non-REM EMs and 3 REM EMs, then a sliding SVM classified the whole sequence of EMs. For sleep phase classification, no models were discarded. The model giving the best classification result was chosen for each type of data (hippocampal recordings and scalp EEG).

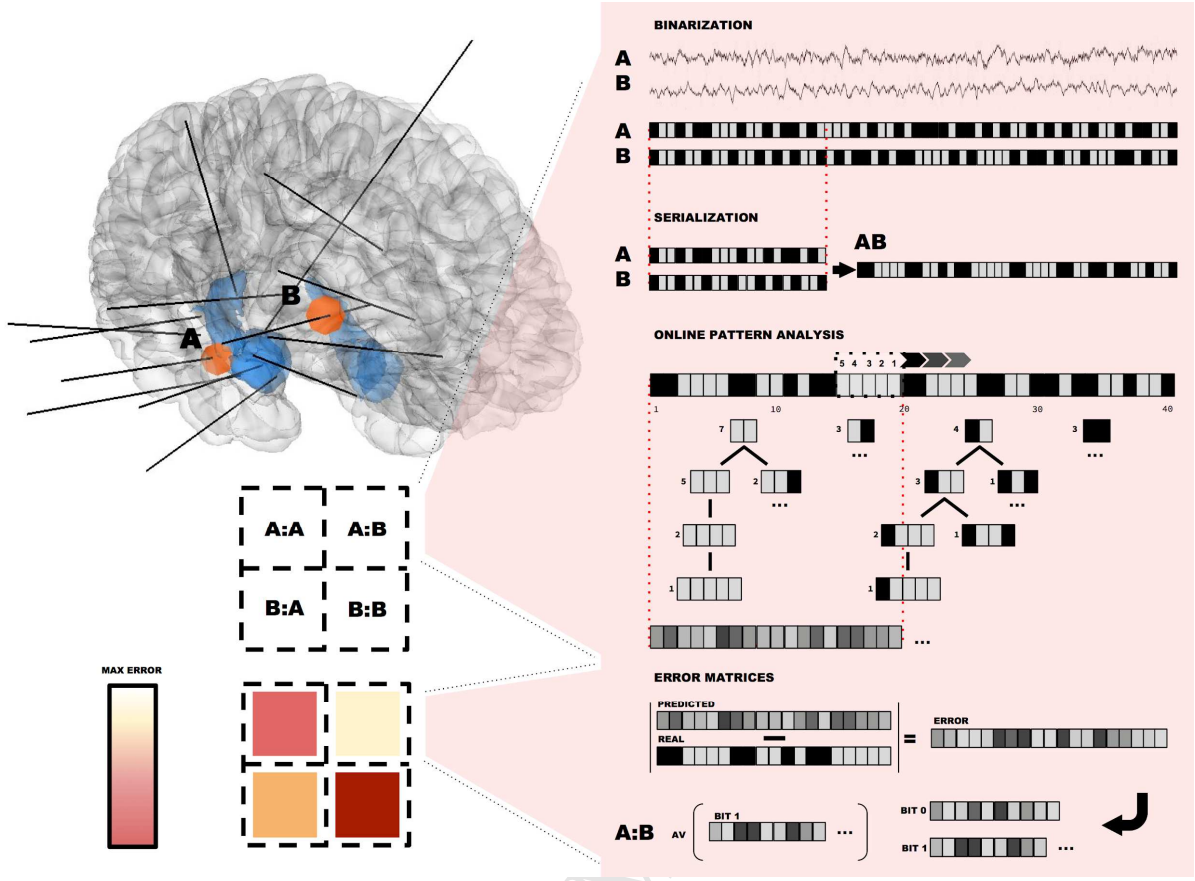

Figure 2. *Prediction error connectivity (PEC) overview*. PEC analyses node pairs and build error matrices (EMs), similar to correlation matrices (see section 2.2 for further details). In the example we show only two contacts taken from a patient with deep electrodes. The analysis can be performed on all or a selected set of contacts. PEC analysis relies on a variable-markov model algorithm (the additive weighted context, AWC) that learns and predicts patterns produced by signal pairs. The method uses the error calculated after predicting the trend of serialized pairs. The notch filtered EEG is processed in four different steps: binarization, serialization, online pattern analysis and the calculation of the error matrices. Briefly, **binarization** transforms the EEG signal in a binary trend or a sequence of bits, **serialization** produces a common output from region pairs to check for synchronization, while the **online pattern analysis** produces a predicted stream, which is compared to the real stream for determining the error rates that are recorded in **error matrices** (refer to sections 2.1 and 2.2 for more details). Note: in the figure we only represent the most common trees and branches found up to position 20 of the AB stream using a context of 1x5 for graphical reasons.

3. Results

PEC is a method that relies on a variable-order Markov model algorithm designed for pattern prediction (the AWC, see section 2.1). In figure 1, we depict an example of text and EEG analysis. The text recorded in unicode characters is the product of 8 synchronous bit streams that generate bitmaps (see figure 1). Similarly, electroencephalographic data recorded from 8 contacts of iEEG is transformed into bitmaps. The AWC transforms bitmaps into probability maps. The latter can be compared to the original bitmaps to obtain error maps. Frequent sequences of characters or EEG patterns are easily predictable and therefore lower the average error. On the other hand, non synchronous or random bit sequences raise the error rates. Using error maps, it is possible to highlight which is the stream responsible of the error increase. Indeed, we generated peaks in error maps by

altering a single bit row with random bit sequences in both text or iEEG data (see figure 1, STREAM ALTERATION).

Apart from the artificial peaks, the first iEEG bit stream shows spontaneous high error rates. In fact, the stream represents the discretized activity recorded from a SOZ channel. This is in line with the hypothesis that an epileptogenic node dynamics would intermittently (e.g. Sinha *et al.*, 2017) or constantly (e.g. Warren *et al.*, 2010) differ from the physiological dynamics of the rest of the network.

Analysing all or several contacts at the same time, like in figure 1, and their combinations would require an unmanageable amount of time and memory, for this reason we devised PEC to analyse node pairs and build error matrices (EMs), similar to correlation matrices. To save time and memory we implemented a very simple transform that solely considers the EEG vector direction (see section 2.2).

The memory requirements were extremely low (around 2 kilobytes per contact pair) and the processing times rather fast: a pair of 10 seconds (5000 points at 500 Hz sampling rate) was processed in 551±39 ms against the 3.84 s ± 92 ms of the pure Python implementation of coherence matrix (CM), while a pair of 60 seconds (30,000 points) was processed in 4.3 s ± 116 ms against the 4 mins 20s ± 12.8 s of CM.

3.1 PEC measures network transitions better than spectral coherence

To create a model where we could control stationarity we generated virtual networks made of five streams. In two of them a variable number of nodes were produced with a linear drift that forced two different dynamics at the start and at the end of a signal. Three conditions were evaluated, a transition from normal to normal, from normal to interictal and from normal to ictal dynamics. In figure 3.B there are examples of these three conditions. A total of twenty hours of virtual EEG signals were generated and divided in epochs of 5x60 streams·seconds, using common nodes (represented as grey circles in figure 3.A) and extra nodes (represented as coloured circles) for each stationary (S) stream. Common nodes and time shifting nodes (orange to red circles) were used for variant (V) streams. Since the proposed method is a network approach, we wanted to simulate a focal change of dynamics and altered the stationarity of 2 among 5 signals. To compare PEC and spectral coherence in detecting transitions the distance (□) between EMs and CMs obtained from the first and the last 30 seconds was calculated. Both whole matrices and the difference between V subnetworks only (all and V in figure 3.B) were considered.

PEC relative changes were more pronounced than those of spectral coherence in all transitions, when considering all conditions like the number of nodes and EEG sub-bands together. In figure 3.B we show the overall results of transition analysis. Interestingly, □EM values almost always defined clear-cut groups, thoroughly distinguishable from □CM groups. Moreover, the difference between whole matrices and V subnetworks were less marked using PEC instead of coherence, therefore suggesting a more robust detection of transitions of similar dynamics. When the transition was driven by two completely different dynamics (from normal to ictal) PEC showed a marked difference between whole EMs and V subnetworks, thus suggesting an enhanced sensitivity to a thoroughly different dynamics, as seen in the *context alteration* experiment. All differences between □EM and □CM were statistically significant ($p < 10^{-6}$).

Also when considering conditions separately, like the ratio between common and variant nodes and sub bands, PEC changes were generally more pronounced than those measured by coherence. However, it was possible to always define clear-cut groups only in broadband.

Interestingly, clear-cut groups were also definable in ripple band, but only in normal and interictal transitions or when considering V subnetworks (see section 7 and table S1 in supplementary materials for condition and band results).

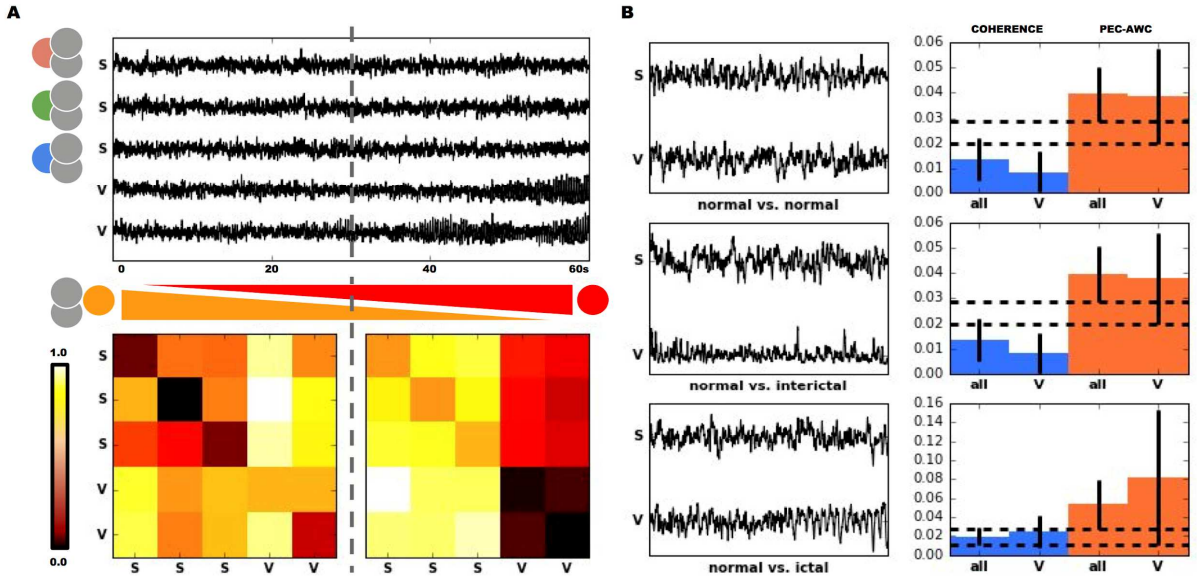

Figure 3. *PEC (red) can distinguish network transitions better than spectral coherence (blue).* **Panel A**. Top: example of virtual focal seizure. We created 20 hours of virtual signals divided in epochs of 5x60 nodes·seconds. Signals were either stationary (S, generated by common and extra nodes -grey and coloured dots respectively- all stable through time) and variant (V, generated using common and time shifting nodes -orange to red dot) with unequal ratios (3:2). Bottom: error matrices (EMs) calculated by the AWC algorithm. We compared the first and the last 30 seconds of the transition. **Panel B**. *Left column*: examples of the three state conditions of V signals that shift from normal to normal excitatory/inhibitory gain (top), from normal to interictal-like (increased excitatory gain, middle) and from normal to seizure-like (increased excitatory, decreased inhibitory gain, bottom). *Right column*: distance between matrices using coherence (blue) and PEC (red), by comparing either whole matrices (all) or V sub-networks. Dotted lines divide the space from each EM average - σ.

3.3 Seizure risk assessment

After verifying that PEC can effectively distinguish virtual network transitions we related EMs to real network states. We considered interictal and preictal states. Despite there is no clear temporal definition of the latter, most of studies consider the preictal period to peak around 30-10 minutes before a seizure (for a review, van Mierlo et al., 2014). Similar temporal limits have been recently used for seizure prediction competitions (Brinkmann et al., 2016). The most successful solutions in these competitions used frequency domain EEG preprocessing and machine learning classifiers ranging from SVM to distributed gradient boosting algorithms. In our study, instead of classifying discrete EEG epochs of binary events, e.g. 10 minutes epochs labeled either as preictal or interictal time, we built a scenario in which we imagined to set a device that continuously samples the EEG, either unabridgedly or with gaps. Initially, a SVM was trained with interictal and preictal EMs calculated from random small samples (only 2 seconds per minute). This allowed to obtain EMs of many nodes (151) in a reasonable amount of time. Risk curves were built by sliding the classifier along the EEG (see section 2.5 for more details, and figure 4.A for a graphical description of the method).

In figure 4.C we present the results using PEC (red) and spectral coherence (blue). Both methods predicted high risk in a variable period of time before the ictal event. However, coherence risk values peaked after the seizure, while PEC predicted the highest risk before

it. We used an arbitrary threshold of 90% (dotted black line). No other peaks were recorded in the considered period of time (4 hours). In figure 4.C the correlation matrix corresponding to the distance between matrices (□EM) used for training the SVM is shown. The most altered lines correspond to the hippocampal head (Hh) and amygdala (Am), which showed interactions with the entorhinal cortex (ERC), the frontal operculum (Fop) and the frontal polar cortex (FPC).

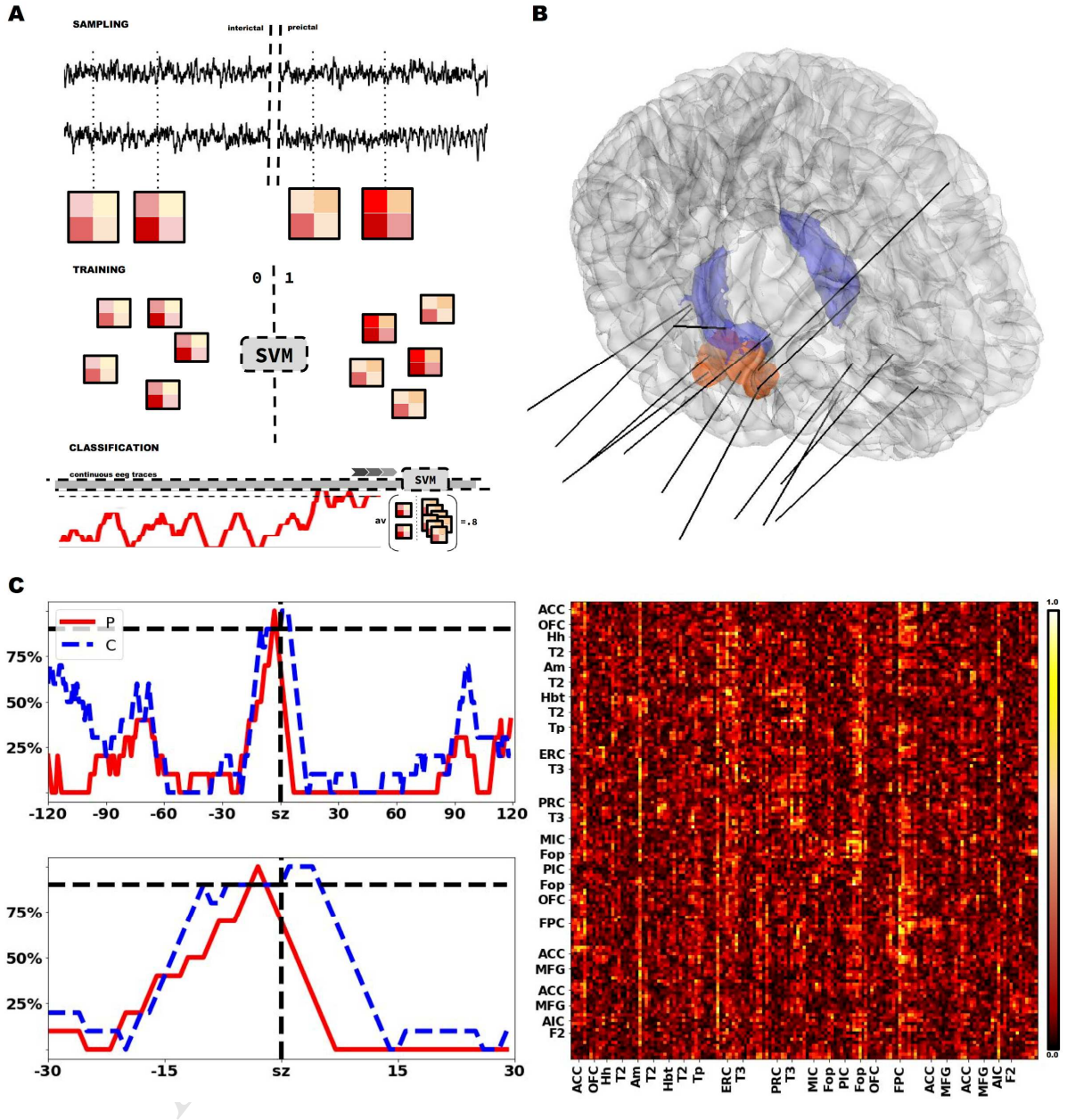

Figure 4. *Seizure risk assessment*. **Panel A.** For risk assessment we used an interictal and preictal period (5 to 10 minutes before the event). After sampling we trained a support vector machine (SVM) to recognise interictal and preictal EMs, scored with 0 and 1 respectively. Finally, the trained SVM classifies continuous EEG data processed into EMs or CMs. A seizure risk curve is obtained by averaging a buffer of 10 matrices -all zeroes, no risk at all; all ones, maximum risk). **Panel B**. *Brain glass model and implants*: the black lines represent the electrodes, the SOZ contact pairs are shown in red. **Panel C**. *Left*: *seizure risk curves* obtained with coherence (C, blue discontinuous line) and PEC (P, red). *Right*: *distance between the EMs* (□EM) used for training the binary classifier. We used distance as a surrogate of the difference between dynamics (interictal vs. preictal) recorded in the explored regions. *Legend*: *ACC*, anterior cingulate cortex; *OFC*, orbitofrontal cortex; *Hh*, hippocampal head; *T2*, 2nd temporal gyrus; *Am*, amygdala; *Hbt*, hippocampal body and tail; *Tp*, temporal pole; *ERC*, entorhinal cortex; *T3*, 3rd temporal gyrus; *PRC*, perirhinal cortex; *MIC*, middle insular cortex; *Fop*, frontal operculum; *PIC*, posterior insular cortex; *FPC*, frontopolar cortex; *ACC*, anterior cingulate cortex; *MFG*, middle frontal gyrus; *AIC*, anterior insular cortex; *F2*, 2nd frontal gyrus.

3.4 Continuous risk assessment by a hypothetical device

Since PEC captured real state transitions from the interictal to the preictal phase we built seizure prediction models simulating a real life application. Models were built always by training the classifier with a single event. To avoid any statistical biases of random sampling in a long time unit (e.g. seconds in a minute), unabridged minutes at the maximum sampling rate were considered. To reduce the processing time and set up a realistic scenario the analysis was restricted to SOZ contacts. By seizure analysis, we identified three contacts recording from three distinct areas of the hippocampal structure: the *cornu ammonis* (CA) region one, three and four (as depicted in figure 5). Afterwards, 1151 minutes of continuous EEG recordings were transformed in two sets of 1151 EMs and CMs, which were used to train 1000 models that predicted all events.

Both CMs and EMs allowed the definition of 1000 risk models that successfully predicted 6 of 7 seizures (we did not count the training event as a predicted event). In figure 5, we present risk curves obtained with spectral coherence (blue) and PEC (red). In the same figure we show EM or CM *best single correlation* (below the risk curves), determined as the maximum value of □CMs and □EMs of the best 10 models. Using spectral coherence we identified the intersection between CA1 and CA3, while using PEC the highest transition changes were determined by the correlation between CA3 and CA4. The *best single correlation* analysis might be used as a fast seizure detection method, since highest coherence values and lowest PEC values corresponded to ictal events. Averaging peri-ictal windows (1 hour before and 1 hour after the seizure) of the *best single correlation*, we graphically assessed the signal-to-noise ratio (SNR) of both methods. PEC clearly surpassed coherence in both seizure risk prediction, and *best single correlation*, as shown by the lower SNR and the fewer threshold curve hits.

In order to quantify these differences, we calculated the effective seizure free-time predicted by an hypothetical device recording from deep electrodes. The number of false warnings and their duration were also assessed. The first 100 models obtained using EMs predicted a considerable higher number of minutes of seizure-free time than models obtained with CMs ($p<0.001$). However, the greatest differences were found by comparing the best 10 models of 1000. PEC reached a top of 1069 minutes of true seizure-free time, which corresponded to the 96% of time in which the patient did not suffer a seizure or its consequences (we considered that each seizure lasted an average of 5 minutes, since 4 of them ended as secondary tonic-clonic and lasted longer than average focal cognitive seizures). Spectral coherence only reached 83%. The group of best PEC models was clearly different from the group of best coherence models ($p<0.0001$) since all PEC models overcame the limit of

1000 minutes, while no coherence model reached that limit. In term of false warnings, again PEC outshone coherence since EM risk curves predicted false events almost two times less frequently than CM models ($p<0.0001$). PEC and coherence models presented comparable average warning times of around 5 minutes.

Finally, we extended this simulation to other four patients with different type of epilepsy and well defined SOZ. In order to avoid comparison biases, again three adjacent SOZ contacts of a single electrode were used to build 1000 models predicting all seizures, after training with a single, randomly selected, ictal event. The best model was selected. PEC allowed the prediction of a total of 27 events distributed in 7 and a half days (10807 minutes, 3,6 seizures per day) in 5 different patients. ROC AUCs reached 98% (average 94%±5%). A total of 8515 minutes (5,9 days) were successfully predicted as seizure-free, corresponding to 80% of all recorded non-seizure time. A total of 244 warnings were issued, corresponding to 8 false warnings per seizure. The average warning time was of 14,3 minutes, ranging from 1 to 168 minutes. Table 1 summarises results per patient.

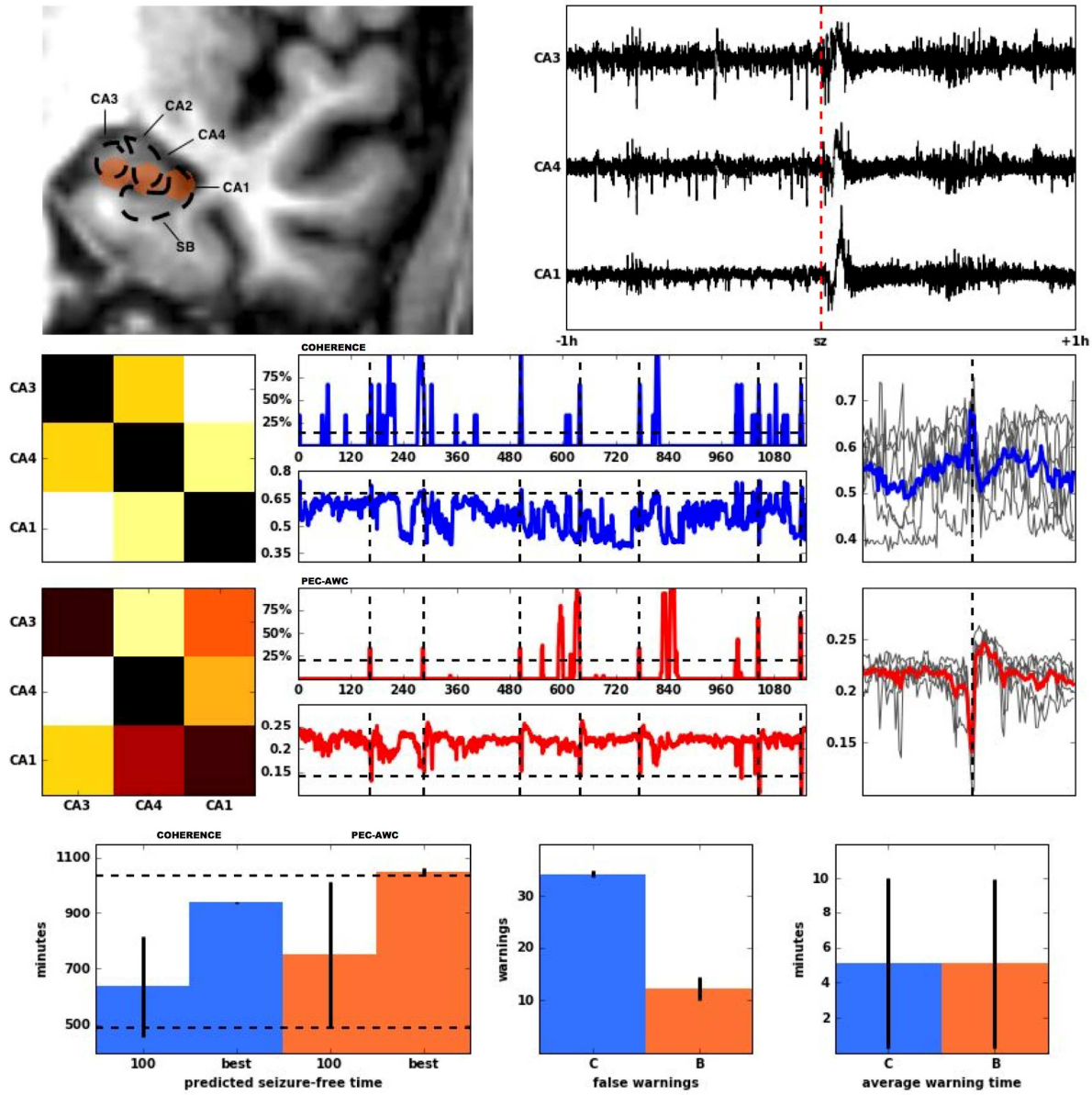

Figure 5. *Continuous risk assessment using SEEG signals*. **Top left**. Epilepsy subject brain MRI, T1 3D sequence. Red translucent circles identify the SOZ: three contacts recording from corpus ammonis (CA) 1, 3 and 4. **Top right**. Continuous SEEG signals 1 hour before and after the first seizure (sz). **Middle left**. CM (top) and EM (bottom) of the best 10 of 1000 models. **Middle centre top**. Seizure risk (up) and best single correlation (C1-C4, down) determined by spectral coherence. **Middle centre bottom**. Seizure risk (up) and best single correlation (C3-C4, down) determined by PEC. **Middle right**. Averaged *best single correlation* of all seizures using 2-hour windows (1 hour before and after the ictal event, marked as a dotted vertical line) using spectra coherence (top) and PEC (bottom). **Bottom**. Predicted true seizure free time using the first 100 and the best 10 models (left). False warnings (centre). Average warning time (left).

	Hippocampal	Temporal	Parietal	Occipital	Frontal
Sex	F	F	M	M	M
Personal history	Unremarkable	Unremarkable	Intellectual disability	Head traumatism	Unremarkable
Duration of epilepsy in years	23	10	38	5	37
Seizure frequency (episodes per year)	100	20	80	50	100
Aura	Epigastric aura and choking sensation	Fear sensation and/or epigastric aura	None	Photopsia	None
Ictal signs and symptoms	Loss of contact, oral and manual automatisms; in the past secondary tonic clonic evolution	Loss of contact, grimace of terror and teeth grinding, then verbal assault and spitting, finally confusion; rare tonic-clonic evolution	Behavioural arrest followed by loss of contact, oral and manual automatisms; half of the times tonic-clonic evolution	Aura followed by subjective vertigo; half of the times loss of contact and ictal speech; rare asymmetrical tonic-clonic evolution	Upward gaze deviation and inverted U grimace, elevation of both arms with slight left predominance, tonic clonic evolution
MRI	Hippocampal sclerosis	Normal	Normal	Extensive R parietal and occipital gliosis	Normal
Interictal PET	R temporal and frontal hypometabolism	R temporal hypometabolism	R frontal and temporal hypometabolism	Extensive R parietal, occipital and temporal hypometabolism	N/A
SISCOM	N/A	R temporal hyperperfusion	R posterior temporal hyperperfusion	R occipital hyperperfusion	R frontal pole hyperperfusion
Electrodes (left)	15 (1)	5 (0)	11 (1)	10 (0)	9 (0)
Surgery Outcome	Engel 1A	Engel IA	Engel II	Engel IA	Engel ID
Pathology	HS	FCD type IA	FCD type IC	Gliosis	Gliosis
Hours analysed (mins)	19,2 (1152)	26,3 (1576)	48,1 (2887)	38,6 (2316)	47,9 (2876)
Seizures (tonic-clonic)	7 (4)	8 (4)	5 (4)	3 (0)	4 (4)
Hours of seizure-free time (mins)	18,4 (1103)	24,0 (1437)	29,4 (1765)	31,4 (1881)	38,8 (2329)
False warnings	10	19	113	63	12
Warning time in mins (min-max)	5,1 (1÷21)	5,1 (1÷19)	15,2 (1÷72)	8,7 (1÷31)	37,6 (1÷168)
ROC AUC	98%	98%	84%	95%	96%

Table 1. *Clinical data and continuous seizure risk assessment*. HS stands for hippocampal sclerosis, FCD for focal cortical dysplasia.

3.5 Continuous risk assessment with downsampling and far from the SOZ

Extending 3.4, we selected a subject without a clear definition of the SOZ. The patient, 42 years old, male, presented seizures with a parietal opercular semiology since he was 27. The MRI was normal, while the PET scan suggested a left insular hypometabolism. Despite the multimodal exploration and the placement of 16 electrodes (170 contacts) we could not record a clearcut SEEG pattern of a focal cortical dysplasia or any other lesion (Lagarde et al., 2016). After the study, surgery was discarded. For this reason we considered the patient as a potential candidate for a hypothetical device designed to send warnings about seizure risk, or a smart electrical stimulator switching on at risk peaks. After the suspension of the medication the patient presented six seizures, only one with tonic-clonic evolution. From recordings, we selected three consecutive days, during which the subject presented four seizure (the last tonic-clonic). We discarded other days because of other clinical tests that involved potentially biasing procedures like electrical stimulation or proximity to the surgical placement of electrodes and the waning of anesthesia. In the selected period the percentage of interictal time reached 99,5%, very close to what is considered the average amount of interictal time of subjects with drug-resistant epilepsy (Andrzejak et al., 2009).
Using the three contacts where the most intense beta/alpha activity preceding a seizure was recorded, it was possible to predict all seizures and 72% of interictal time (86% ROC AUC) totalling 3102 minutes. There were 253 false warnings, the minimum warning time was 1 minute, the maximum 130 minutes, the average 10 minutes and 29 seconds. By downsampling to 62 Hz and using the first two seconds of each minute, the prediction of interictal time fell to 68% (84% ROC AUC) totalling 2929 minutes. There were 341 false warnings, the minimum warning time was 1 minute, the maximum 130 minutes, the average 9 minutes and 26 seconds. Interestingly, by downsampling to 62 Hz and using three hippocampal contacts, a region away from the suspected SOZ and unaffected by interictal activity, the interictal time prediction rose again to 72% (86% ROC AUC) totalling 3136 minutes. There were 310 false warnings, the minimum warning time was 1 minute, the maximum 70 minutes, the average 5 minutes and 38 seconds.

3.6 Sleep phase transition classification

As a final extension, non-REM to REM phase transitions were classified using hippocampal and scalp EEG recordings. A night recording (8 hours and 55 minutes) from the same subject of 3.5 was used. In this patient hippocampal interictal activity was ruled out and the scalp EEG recordings were taken from the unaffected hemisphere. Non-REM to REM transitions were considered instead of interictal to preictal transitions, the same framework of 3.4 and 3.5 was used. A model built with just six EMs (3 taken in non-REM phases and 3 taken 1 to 3 minutes before a REM phase) processed from hippocampal recordings correctly classified 88% of the considered time (91% for REM, 86% for non-REM). Accuracy fell to 81% using scalp EEG recordings (72% for REM, 90% for non-REM). Interestingly, in both cases -although more clearly with hippocampal recordings- curves not only distinguished REM from non-REM phases, but could actually anticipate the phase transition (Figure 6).

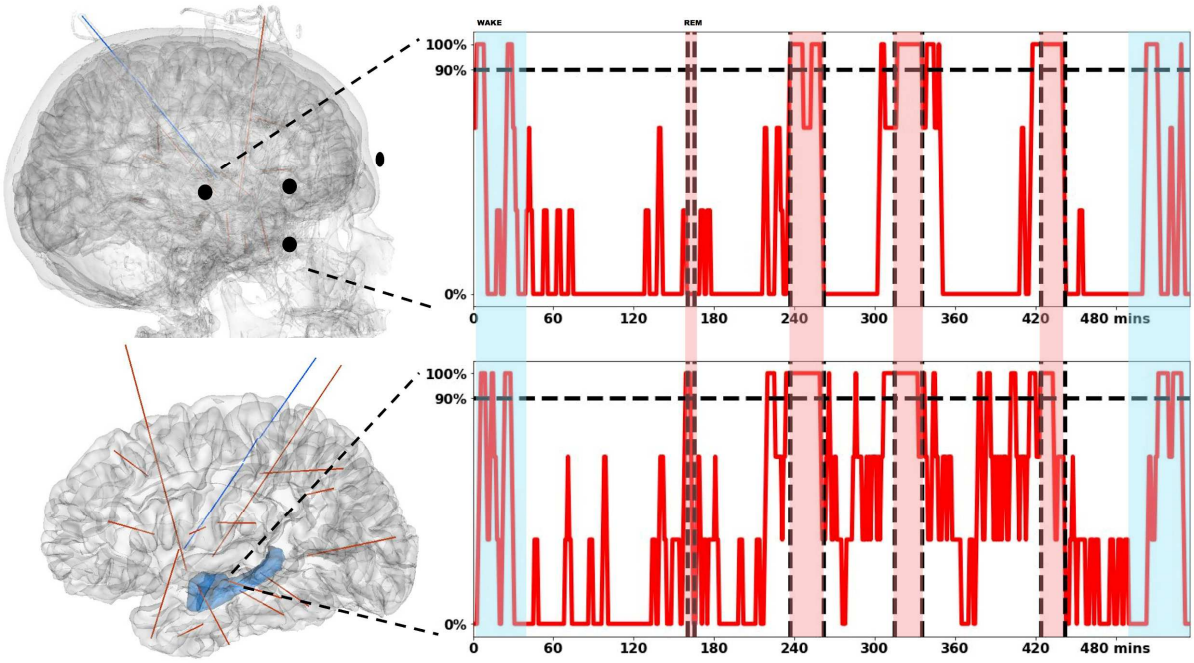

Figure 6. *Sleep phase transitions anticipated by PEC*. The sleep phases were staged in a 535 minutes night recording in a patient implanted with deep electrodes and recorded both from deep and scalp contacts. The classification was done using PEC by considering the REM phases as seizures (periods longer than 5 minutes were divided in multiple, contiguous events), 1000 models were trained, no model was discarded. REM phases are marked by discontinued vertical lines and a red transparent overlay, while the blue transparent overlay marks wake periods. **Top**. Scalp electrode classification: 72% of REM was correctly classified, ROC-AUC 81%. **Bottom**. Hippocampal classification: 91% of REM was correctly classified, ROC-AUC 88%. Note: electrode implants on the right hemisphere are depicted in blue, on the left in red.

4. Discussion

In this work we introduce a novel approach to measure network state transitions. The prediction error connectivity (PEC) infers dynamics changes from their predictability. Like other markovian methods modeling relations and dependence between channels (e.g. Wulsin et al., 2014), PEC as well predicts interactions between channels (EEG sources). Unlike other measures, PEC uses the prediction error to infer dynamics changes. Another point of novelty provided by our work is the implementation of such concept through a new algorithm, the Averaged Weighted Context (AWC), which we proved effective for data compression. Finally, a third important difference between PEC and other approaches, is the characterisation of dynamics states by just using the direction of the electric vector, thus requiring very low memory and processing times.

To test PEC we first measured controlled transitions of signals produced by neural masses already described to effectively produce virtual iEEG signals. We generated virtual networks with stationary (S) and variant (V) signals. PEC distinguished whole virtual network and V subnetwork transitions better than spectral coherence, regardless of the type of transition. Interestingly, PEC not only showed to be more effective than coherence but also more robust, since measures obtained with whole virtual networks did not differ much from values obtained with V subnetworks when the transition occurred between similar dynamics. This finding suggests that the method specifically captures the transition and is only slightly modified by stationary dynamics.

The only exception were the transitions from normal to ictal states. Whole network differences in this case were more attenuated in comparison with V subnetwork changes, even more than in coherence dependent measures. This might be due to the ictal dynamics themselves, which are more regular and therefore represented, as shown in figure 3.A, by more stable subnetworks. Indeed in the $EM_{30\text{-}60s}$ displayed in the figure, the error values of V ictal signals are the network lowest. This is in line with the findings obtained with the seizure risk assessment. In that part of the work performed with real data, we verified that error rates drop during seizures, as shown by *best single correlation* plots (see Figure 5). The latter represented the most relevant interaction between hippocampal areas before and during seizures. To single out these interactions we compared the matrices used to successfully train a SVM classifier to assess the seizure risk, which implies a correct classification of transitions between interictal and preictal states. PEC demonstrated higher performance than spectral coherence in terms of true seizure free time and amount of false warnings. In other words, both methods allowed the generation of models that captured the interictal-preictal state transitions, but PEC showed higher specificity than coherence. Interestingly, as shown by the *best single correlation* plots, PEC performed better detecting ictal events. Nonetheless, as expected, it showed the opposite trend than coherence on seizures. Unexpectedly, however, it allowed better SNR hence supporting a potential application in seizure detection.

Apart from pathological state transitions, we also demonstrated that PEC can classify and even forecast REM sleep phases. This finding suggests that the algorithm usage might be extended to the analysis of neuropsychological data. The concept behind PEC does not either fit, nor is in contrast with any of the models conceived for explaining the mechanisms behind interareal information processing. First of all, the measure considers exclusively the temporal domain, therefore there are no constraints about selected frequencies, or any frequency at all, since the frequential information is translated into pattern matching. Indeed, the model conceives frequencies as patterns that repeat over time. When comparing to the hypothesis of communication through coherence, PEC certainly contemplates synchronization, but it actually checks about repetitive patterns formed by the interplay between two areas. Although synchronic, these patterns might not be either coherent (in terms of the physical measure) nor display the same or similar frequential composition. PEC just predicts patterns that are the result of the arrangement of two brain areas dynamics, blind to their covariance or phase lock. In other words, it does not matter how complex the pattern is or within which sequence it is repeated, when it is encountered twice or more times, the prediction is feasible. For this reason, the PEC approach might yield lower error values when two brain areas are phase locked transiently, covariate, or even when such alternate slow and high frequency activity. Therefore coupling this measure with other frequential methods might add depth to current connectivity analyses. Another potentially interesting feature of PEC for cognitive studies is its ability to produce asymmetrical connectivity matrices, as shown in figure 3, 4 and 5. This characteristic that implies directionality (the pair AB might be easier to predict that the pair BA) should be investigated further, compared with causal measures like Granger causality or regression analysis, and validated with cognitive studies that involve known and unknown causal relations between brain areas.

Considering seizure prediction applications, the method allowed us to continuously analyse 10,5 days of iEEG and predict 31 seizures with average ROC AUC of 93%. Most relevantly, this corresponded to correct a prediction of 82% of all non-seizure time, which is used by patients for social and personal activities. In this introductory analysis we just discarded models that failed to predict all seizures, which would be impossible in a real scenario. Nonetheless, we demonstrated that it is possible to build 1000 different models per 42 hours of average recording time, which predict an average of 5 seizures using a single event for training. In future studies, using whole recording times (weeks of recording), we will calculate seizure and seizure free-time prediction rates using incremental datasets by simulating scenarios of data acquisition and new event prediction and detection. With the experiment described in 3.5, we hint at the possibility that even abridged and low sample recordings might allow a good classification of interictal time. This result, along with PEC low memory footprint and processing speed, suggests that the algorithm could be successfully implemented in a portable, low-power consumption device, and that further battery time could be saved by low sampling rates and sparse recordings. The hippocampal recordings, on the other hand, show that such hypothetical device might work even with implants placed far from the SOZ.

Our study presents several limitations and its findings are still far from being used to produce real life applications or to be whatsoever generalised. First of all, the central idea about pattern analysis and brain dynamics should be experimentally confirmed, possibly with animal models, local field potentials and single neuron recordings. Moreover, in this setting we should also perform several other comparisons, especially with derivatives of spectral coherence and other synchronicity measures.

From a neuroscientific point of view, despite the promising results obtained with REM sleep, PEC will need to be tested on other clinical and neurophysiological settings before being considered a useful tool. Further studies should compare it with other, more established analysis methods. In this study we only hint at the potential applications of the PEC approach. For instance, connectivity matrices considering interactions between three or more nodes are only briefly discussed in the methods of our manuscript (see the stream alteration test and the comparison between text and iEEG datasets), but not explored in detail. In cognitive studies, where processing time and memory are not crucial, the exploration of channel combinations might give insights about the ordered processing of brain areas and the causal relationship between them. Moreover, this introductory study only contemplates shape (the direction of the electrical vector) as input, discarding amplitude information. Further studies should take into account other binarization and discretization options, like wavelets.

In the clinical domain, despite the good predictability shown for different types of epilepsy and across different brain regions, recordings from more patients will be needed to further confirm the potential of this tool. Although our study suggests that few adjacent contacts from a single electrode could be sufficient to build prediction models, the optimal number of contacts and their relation to the SOZ and/or epileptogenic zone remains to be fully assessed. Indeed, that fact that seizures could be anticipated by using recordings from a healthy brain region away from the SOZ suggests that seizures are a phenomenon triggered by the interaction between their generator and the rest of the network. Which are the main actors and whether all brain regions participate in this interaction are interesting questions still to be answered. From another point of view, it would be very interesting to know whether it is necessary to target the SOZ in order to forecast ictal events, since in many patients

surgery is discarded precisely because of the lack of definition of the SOZ. Indeed these would be the target patients of such alternative strategies. Finally, to consider real life applications, it will be necessary to robustly assess predictability with low sampling rates and sparse recording strategies, extending these tests to other patients and several hours/days of recordings.

In conclusion, PEC is a novel variable-order Markov-chain approach that can be used in the study of epilepsy and likely any neuroscientific studies involving the analysis of EEG and iEEG. We demonstrate that PEC is superior to spectral coherence (and possibly other frequential measures) in assessing network dynamics transitions and we suggest that our method might be successfully implemented to power a device employed for seizure prediction. Although preliminary, these results are encouraging and might lead to the creation of new strategies and algorithms that might add up to existing ones already used in implantable (Cook et al., 2013) or upcoming devices.

5. References

Aarabi A, He B. A rule-based seizure prediction method for focal neocortical epilepsy. Clinical Neurophysiology. 2012 Jun 1;123(6):1111-22.

Aarabi A, He B. Seizure prediction in patients with focal hippocampal epilepsy. Clinical Neurophysiology. 2017 Jul 1;128(7):1299-307.

Andrzejak RG, Chicharro D, Elger CE, Mormann F. Seizure prediction: Any better than chance?. Clinical Neurophysiology. 2009 Aug 1;120(8):1465-78.

Audit B, Vaillant C, Arnéodo A, d'Aubenton-Carafa Y, Thermes C. Wavelet analysis of DNA bending profiles reveals structural constraints on the evolution of genomic sequences. Journal of Biological Physics. 2004 Mar 1;30(1):33-81

Baldassano S, Wulsin D, Ung H, Blevins T, Brown MG, Fox E, Litt B. A novel seizure detection algorithm informed by hidden Markov model event states. Journal of Neural Engineering. 2016 Apr 21;13(3):036011.

Brinkmann BH, Patterson EE, Vite C, Vasoli VM, Crepeau D, Stead M, et al. Forecasting seizures using intracranial EEG measures and SVM in naturally occurring canine epilepsy. PLoS One 2015; 10: e0133900

Brinkmann BH, Wagenaar J, Abbot D, Adkins P, Bosshard SC, Chen M, Tieng QM, He J, Muñoz-Almaraz FJ, Botella-Rocamora P, Pardo J. Crowdsourcing reproducible seizure forecasting in human and canine epilepsy. Brain. 2016 Jun 1;139(6):1713-22.

Buzsáki G, Anastassiou CA, Koch C. The origin of extracellular fields and currents—EEG, ECoG, LFP and spikes. Nature Neuroscience Reviews . 2012 Jun 1;13(6):407-20.

Cook MJ, O'Brien TJ, Berkovic SF, Murphy M, Morokoff A, Fabinyi G, D'Souza W, Yerra R, Archer J, Litewka L, Hosking S. Prediction of seizure likelihood with a long-term, implanted seizure advisory system in patients with drug-resistant epilepsy: a first-in-man study. The Lancet Neurology. 2013 Jun 30;12(6):563-71.

Cortes C, Vapnik V. Support-vector networks. Machine Learning. 1995 Sep 1;20(3):273-97.

Dadok VM, Kirsch HE, Sleigh JW, Lopour BA, Szeri AJ. A probabilistic method for determining cortical dynamics during seizures. Journal of Computational Neuroscience. 2015 Jun 1;38(3):559-75.

Fell J, Klaver P, Lehnertz K, Grunwald T, Schaller C, Elger CE, Fernández G. Human memory formation is accompanied by rhinal–hippocampal coupling and decoupling. Nature Neuroscience. 2001 Dec 1;4(12):1259-64.

Hunter JD. Matplotlib: A 2D graphics environment. Computing in Science & Engineering. 2007 May;9(3):90-5.

Jones E, Oliphant T, Peterson P. others. SciPy: Open source scientific tools for Python. 2001. URL http://www. scipy. org. 2016.

Kwan P, Brodie MJ. Definition of refractory epilepsy: defining the indefinable?. The Lancet Neurology. 2010 Jan 1;9(1):27-9.

Lagarde S, Bonini F, McGonigal A, Chauvel P, Gavaret M, Scavarda D, Carron R, Régis J, Aubert S, Villeneuve N, Giusiano B. Seizure□onset patterns in focal cortical dysplasia and neurodevelopmental tumors: Relationship with surgical prognosis and neuropathologic subtypes. Epilepsia. 2016 Sep 1;57(9):1426-35.

Langmead B, Trapnell C, Pop M, Salzberg SL. Ultrafast and memory-efficient alignment of short DNA sequences to the human genome. Genome Biology. 2009 Mar;10(3):R25.

Matsumoto JY, Stead M, Kucewicz MT, Matsumoto AJ, Peters PA, Brinkmann BH, Danstrom JC, Goerss SJ, Marsh WR, Meyer FB, Worrell GA. Network oscillations modulate interictal epileptiform spike rate during human memory. Brain. 2013 Jun 25;136(8):2444-56.

Mormann F, Andrzejak RG, Elger CE, Lehnertz K. Seizure prediction: the long and winding road. Brain. 2006 Sep 28;130(2):314-33.

Palmigiano A, Geisel T, Wolf F, Battaglia D. Flexible information routing by transient synchrony. Nature Neuroscience. 2017 May 22.

Pedregosa F, Varoquaux G, Gramfort A, Michel V, Thirion B, Grisel O, Blondel M, Prettenhofer P, Weiss R, Dubourg V, Vanderplas J. Scikit-learn: Machine learning in Python. Journal of Machine Learning Research. 2011;12(Oct):2825-30.

Piggott BJ, Liu J, Feng Z, Wescott SA, Xu XS. The neural circuits and synaptic mechanisms underlying motor initiation in C. elegans. Cell. 2011 Nov 11;147(4):922-33.

Rodriguez E, George N, Lachaux JP, Martinerie J. Perception's shadow: long-distance synchronization of human brain activity. Nature. 1999 Feb 4;397(6718):430.

Santaniello S, Sherman DL, Mirski MA, Thakor NV, Sarma SV. A Bayesian framework for analyzing iEEG data from a rat model of epilepsy. InEngineering in Medicine and Biology Society, EMBC, 2011 Annual International Conference of the IEEE 2011 Aug 30 (pp. 1435-1438). IEEE.

Schulze-Bonhage A, Kühn A. Unpredictability of Seizures and the Burden of Epilepsy. Seizure prediction in epilepsy: from basic mechanisms to clinical applications. 2008 Nov 21.

Sinha N, Dauwels J, Kaiser M, Cash SS, Brandon Westover M, Wang Y, Taylor PN. Predicting neurosurgical outcomes in focal epilepsy patients using computational modelling. Brain. 2016 Dec 30;140(2):319-32.

Stacey W, Le Van Quyen M, Mormann F, Schulze-Bonhage A. What is the present-day EEG evidence for a preictal state?. Epilepsy Research. 2011 Dec 1;97(3):243-51.

van Mierlo P, Papadopoulou M, Carrette E, Boon P, Vandenberghe S, Vonck K, Marinazzo D. Functional brain connectivity from EEG in epilepsy: Seizure prediction and epileptogenic focus localization. Progress in Neurobiology. 2014 Oct 31;121:19-35.

Walt SV, Colbert SC, Varoquaux G. The NumPy array: a structure for efficient numerical computation. Computing in Science & Engineering. 2011 Mar;13(2):22-30.

Warren CP, Hu S, Stead M, Brinkmann BH, Bower MR, Worrell GA. Synchrony in normal and focal epileptic brain: the seizure onset zone is functionally disconnected. Journal of Neurophysiology. 2010 Dec 1;104(6):3530-9.

Wendling F, Bellanger JJ, Bartolomei F, Chauvel P. Relevance of nonlinear lumped-parameter models in the analysis of depth-EEG epileptic signals. Biological Cybernetics. 2000 Sep 1;83(4):367-78.

Wulsin DF, Fox EB, Litt B. Modeling the complex dynamics and changing correlations of epileptic events. Artificial Intelligence. 2014 Nov 30;216:55-75.

Yang T, Gu C, Yang H. Long-Range Correlations in Sentence Series from A Story of the Stone. PloS one. 2016 Sep 20;11(9):e0162423.

Ziv J, Lempel A. Compression of individual sequences via variable-rate coding. IEEE transactions on Information Theory. 1978 Sep;24(5):530-6.